Local Curvature of Turbulent Premixed Ammonia and Blends with Methane and Hydrogen Flames in a Spherically Expanding Configuration

Pierre Brequigny, Seif Zitouni, Christine Mounaïm-Rousselle

Local Curvature of Turbulent Premixed Ammonia and Blends with Methane and Hydrogen Flames in a Spherically Expanding Configuration

S. Zitouni*[1], P. Brequigny[1], C. Mounaïm-Rousselle [1]

[1]Université d'Orléans, INSA-CVL, EA 4229—PRISME, 45072 Orléans, France

Abstract

Local flame structure analysis of NH_3 and blends with CH_4 and H_2 was conducted upon spherical expanding flames, facilitated by the use of Mie-scattering tomography. The wrinkling ratio was found to increase with both increasing NH_3 fraction and turbulent intensity, in agreement with observed flame geometries. Results show that the local curvature pdf of the pure NH_3 flame shifts towards greater local zero curvature with increasing eddy turn over time. In general, the mean curvature is positive for all examined flames, with an increase in turbulence intensity resulting in a widening of the curvature distribution, in agreement with measured wrinkling ratios.

Introduction

The historical prevalence of hydrocarbon fuel usage to sustain our power and transport needs and the associated greenhouse gas emissions produced have resulted in important environmental and ecological adversities [1]. Furthermore, from a European perspective, declining indigenous resources, increased dependence on imports and intermittent renewable energy, have resulted in an increasingly diverse energy landscape. In this context, Ammonia (NH_3) has emerged in recent years as an efficient zero-carbon Hydrogen (H_2) carrier. Although NH_3 offers several advantages (i.e. a high volumetric energy density, a mature global storage and distribution infrastructure [2]) there remains several practical combustion challenges, notably the control and reduction of pollutant emissions (NO_x and N_2O). Moreover, NH_3 exhibits slow burning velocities, long ignition delay times and high auto-ignition temperatures which have restricted wide scale application. To improve NH_3's combustion properties, blending NH_3 with methane (CH_4) (for a partial decarbonization) or H_2 (from the possible 'in situ' cracking of ammonia) has been proposed, and has gained considerable recent attention, with comprehensive reviews of NH_3 related work undertaken [2], [3]. Successful demonstrations in both gas turbines [4], [5] and internal combustion engines [6], [7] have been achieved at high temperatures and pressures.

In literature, the research upon the laminar burning velocity (S_L^0 or LBV), one fundamental physiochemical property of a premixed combustible mixture, of NH_3 based fuels has been increasingly investigated. Work has been undertaken at high temperatures [8], [9], and high pressure [8], [10], [11]. In general, S_L^0 of NH_3 increases linearly with addition of CH_4, whilst an exponential increase is observed with increasing H_2 fraction. An increase in temperature and pressure produces an inhibiting and enhancing effect, respectively, upon S_L^0 of NH_3 and its blends with CH_4 and H_2. However, there remains limited peer-reviewed studies about turbulence-flame interaction for NH_3 fuel, more reflective of practical combustion systems.

Relative to the LBV, the turbulent burning velocity (S_T) is enhanced due to flame stretch and wrinkling induced by the turbulence, with potential enhanced mixing resulting in an increase in combustion efficiency. The very different characteristics of NH_3 flames (low flame speed (S_L^0) coupled with large flame thickness (δ)) relative to hydrocarbons result in significant differences in relative chemical time scales (ratio of $S_L^0/\ \delta$). As a consequence, the turbulent burning of NH_3 leads to higher turbulence Karlovitz numbers (Ka) [12]. Kobayashi et al. [3] and Zitouni et al. [13] showed that adding NH_3 to turbulent CH_4 and H_2 flames results in a larger scale of the wrinkled flame front, potentially due to an increase in the flame thickness with NH_3 addition. Other recent turbulent combustion experiments, underline the role of preferential-diffusion and flame stretch interaction upon NH_3-based turbulent flames [7], [14]. Considerable progress has been made in understanding turbulent NH_3-based combustion, but current understanding of some of the physical phenomena, such as the influence of turbulent wrinkling upon local curvature and local flame speed remains scarce, particularly from an experimental perspective.

In the present study, a large set of flame kernels have been recorded in a near iso-tropic turbulent flow-field in order to study local turbulent-flame interaction. A constant-volume spherical vessel was employed, closely mimicking practical situations such as combustion in engines. Planar Mie-Scattering tomography was utilized to visualize the flame kernel development during propagation in the turbulent flow field. The global wrinkling, as well the local curvature at each step of the flame propagation are evaluated and discussed, with respect to turbulence intensity and mixture composition.

Experimental and numerical methods

Flame measurements were performed using a constant-volume spherical chamber, with the vessel

* Corresponding author: seif-eddine.zitouni@univ-orleans.fr

fitted with six-four blade fans, positioned in a regular hexahedral configuration, producing a near iso-tropic and homogenous region within a radius of 20 mm of the vessel center, fully described in [15]. The non-reacting turbulent flow field within the vessel was characterized by high-speed particle image velocimetry to verify turbulent parameters, namely the turbulent intensity as the rms of the turbulent fluctuation velocity (u_{rms}=u') and the integral length scale (T_L). Minimal changes in the homogeneity and isotropy ratios of the flow field (acceptable range was set to 0.95 and 1.05, ± 5% of ideal case) were observed. It was concluded that u' increases linearly with increasing fan speed (ω), expressed as u'= Af_0, where f_0 = (ω/60) and A, a constant = 0.0098 m. Finally, by means of two-point velocity correlation, in the longitudinal and lateral directions, the integral length scale was found to be insensitive to the rotational speed (2000 – 15000 rpm), remaining almost constant (T_L~2.64 mm), in good agreement with previous work using the same set-up [15].

Two fan speeds were investigated (3000 and 5000 rpm) inducing mean turbulent intensities, u' = 0.49 and 0.82 m/s, respectively. With respect to mixture compositions, the mole fraction of CH_4 in NH_3 was varied as 30%, 60% and 100%, with that of H_2 in NH_3 varied as 10%, 30%, 60%. Measurements for the mixtures were performed at initial conditions of 298K (± 3K) and 0.1 MPa (± 1x10^{-3} MPa). It should be underlined that since at 298 K, the NH_3/air flame due to its very low laminar flame speed would be conveyed away from the measurement plane even at lowest turbulence intensities, the initial temperature was fixed at 423 K to partially resolve this issue, although important losses in sphericity were observable. All experiments were conducted at stoichiometric conditions (Φ = 1.0), with 3-5 nominally identical experiments for each condition, with Table 1 summarizing the laminar and turbulent flame properties of the experimental conditions.

Mie-scattering laser tomography was employed, enabling enhanced precision with respect to flame front wrinkling by the turbulence. Details of this optical set-up alongside the employed post-processing techniques can be found in [16] and thus only a brief summary is presented here. A Dual-Hawk HP Nd:YAG laser was used to illuminate silicon oil droplets, with flame propagation recorded using a Phantom V1610 high-speed camera perpendicular to the laser sheet, set to capture 10,000 fps and facilitating a spatial resolution of 0.0833 mm/pixel. Flame propagation rates were calculated by edge-detection algorithms written in a bespoke MATLAB script. By assuming a spherical flame, from the binarized flame contour images, the surface equivalent flame radius (R_s) and perimeter (R_p), defined as $R_s=(A/\pi)^{1/2}$ and $R_p=(P/2\pi)$, where A represents the burnt gases area and P the perimeter, were determined. The wrinkling ratio (W) was evaluated to be $W=R_p^2/R_s^2$, as defined in [17]. Lastly, the local flame curvature was estimated as follows [18]:

$$h = [x(s)'y(s)'' - y(s)'x(s)'']/[(x(s)'^2 + y(s)'^2)]^{3/2}$$

where $x(s)$ and $y(s)$ the coordinates on the spline curve and s the curvilinear coordinate. For positive flame front curvature, the local flame front is convex towards the fresh gases, with negative values to regions convex toward the burnt gases.

Table 1: Laminar and turbulent flame properties of the experimental conditions at Φ = 1.0 and P= 0.1 MPa.

Description	Pure Fuels		% vol. of CH_4 in NH_3		% vol. of H_2 in NH_3		
(units)	CH_4	NH_3	30%	60%	10%	30%	60%
T_u ± (3 K)	298	423	298	298	298	298	298
[a] δ_L (mm)	0.48	2.03	1.05	0.69	1.57	0.84	0.37
S_L^0 (m/s)	0.363	0.137	0.129	0.210	0.117	0.241	0.665
L_b (mm)	0.642	1.369	1.079	0.868	1.138	0.587	0.073
[b] Le_{eff}	1.01	0.96	0.97	0.99	0.94	0.90	0.80
[c] α (cm^2/s)	0.223	0.292	0.225	0.225	0.238	0.269	0.329
u' (m/s)	0.49-0.82	0.49-0.82	0.49-0.82	0.49-0.82	0.49-0.82	0.49-0.82	0.49-0.82
[d] Ka	0.67-1.45	5.96-12.9	4.64-10.1	1.83-3.96	6.64 -14.4	1.63-3.54	0.24- 0.52
[e] Da	4.07-2.43	0.36-0.22	0.67-0.40	1.63-0.97	0.40- 0.24	1.55- 0.92	9.56-5.71
[f] δ_T (mm)	3.21-3.86	5.57-6.71	4.20-5.58	3.81-5.05	5.04-5.60	3.69-4.77	2.53-3.22

[a] Laminar flame thickness $\delta_L = (T_{ad} - T_u)/(dT/dx)_{max}$.
[b] Effective Lewis number based upon a volumetric fraction weighted average, L_{eff}
[c] Thermal diffusivity of reactants, α.
[d] $Ka = (u'/S_L^0)^{3/2} / (L_T/\delta_L)^{1/2}$
[e] $Da = (L_T/u')*(S_L^0/\delta_L)$
[f] $\delta_T = (u'T_L)^{1/2} \cdot t^{1/2}$, brush thickness, with t, the time measured from ignition event

Results and Discussion

For the present experiments, the turbulent premixed flames were located within the thin reaction regime up to 60% H_2 vol., with that mixture situated within the corrugated flamelets regime, a consequence of a much greater laminar burning velocity. Under the thin reaction regime, the flame still behaves locally as a flamelet for the large eddies, however small eddies are now able to penetrate within the preheat zone of the flame structure, resulting in enhanced mass and heat transfer rates [19], and consequently a 'broadening' of the flame. The reaction zone of the flame remains only wrinkled, since the Kolmogorov scale remains larger than the reaction sheet.

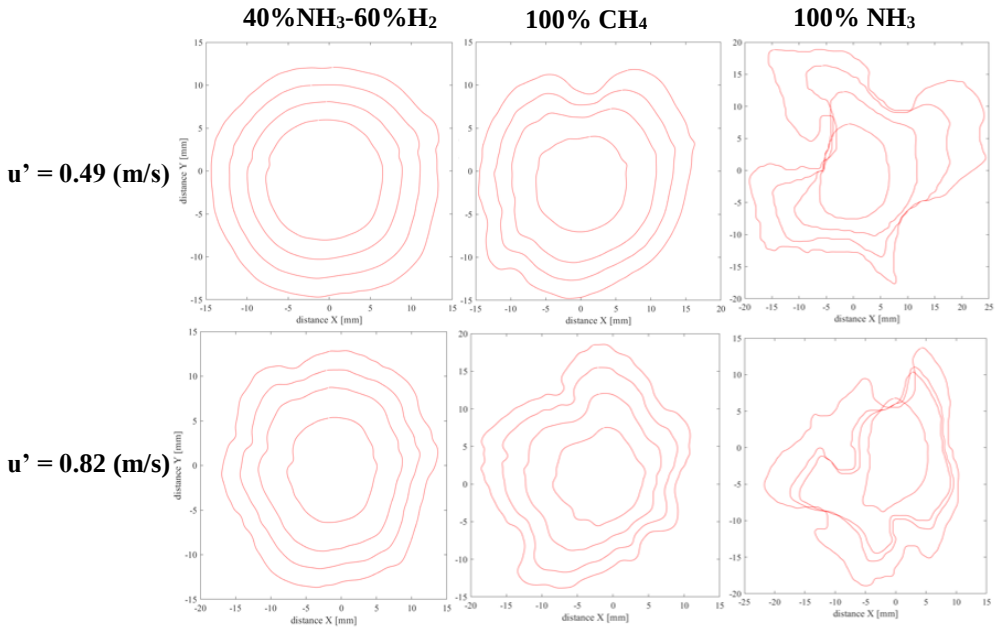

Figure 1: Evolution at various surface equivalent radii (R_s = 5, 8, 10, 12 mm) of a typical stoichiometric 40%NH_3-60%H_2, 100% CH_4 and 100% NH_3 flame.

Due to the homogeneous isotropic turbulent zone for the present experimental set-up, observable flame radii are restricted to 20mm. Moreover, due to the low laminar burning velocities of NH_3 based fuels, some flames were conveyed away from the center of the vessel by large turbulent structures. As a result, the laser sheet did not cut the maximum flame radius resulting in limited range of observable radii. Even though relatively short lengths of flames are available, insightful information is still gained with respect to effects of the turbulent flow field on the flame (in the shape of the flame has adopted in response to turbulent structures it encountered) as well as the influence of flame shape on flamelet burning.

The temporal evolutions of flame contours at equivalent flame radius for stoichiometric 100% NH_3, 100% CH_4 and 40%NH_3 – 60% H_2 at a u' = 0.49 and 0.82 m/s are illustrated in Figure 1. In the case of 100% CH_4 and 40/60% NH_3/H_2 flames, initial stages of flame development (R~5 mm) are similar, with a flame globally laminar, with this observation maintained for both turbulent intensities. With respect to 100% NH_3, the global flame shape is affected at a very early stage of flame development, with clear loss of sphericity. For 100% CH_4 and 40/60% NH_3/H_2 flames, the flame front seems to reach a certain geometry after a certain duration (transition period), maintaining this mean morphology over time, presumably after the flame structure becomes greater than the turbulence structure represented by the turbulent integral length scale, as noted by [17]. For 100% NH_3 flames, the flame geometry keeps evolving with time, with development of elongated 'tube or strip' shapes, with similar morphologies noted by [7], [13]. The amplitude of flame wrinkling is directly influenced by u'/S_L^0, as the highest values of u'/S_L^0, correspond to the least reactive fuels (lowest S_L^0, blends containing the most NH_3), with those mixtures exhibiting flame contours which are strongly distorted and wrinkled by the turbulent flow field.

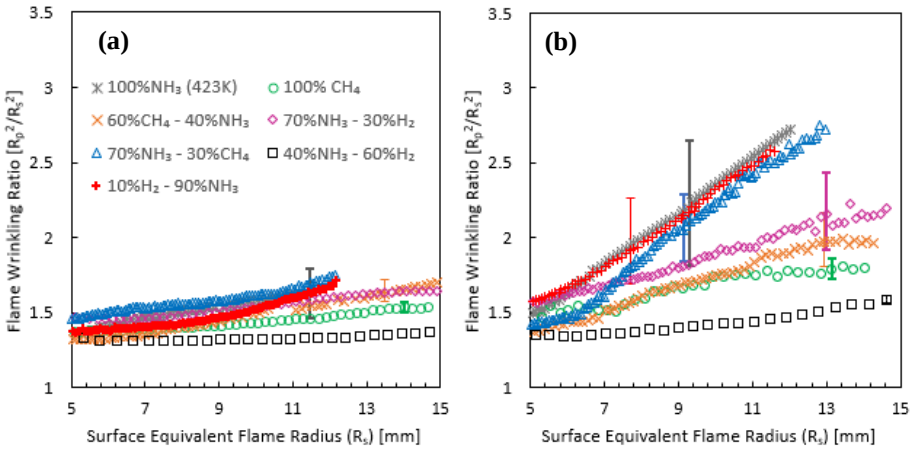

Figure 2: Flame wrinkling ratio as a function of flame radius for (a) u' = 0.49 m/s and (b) u' = 0.82 m/s

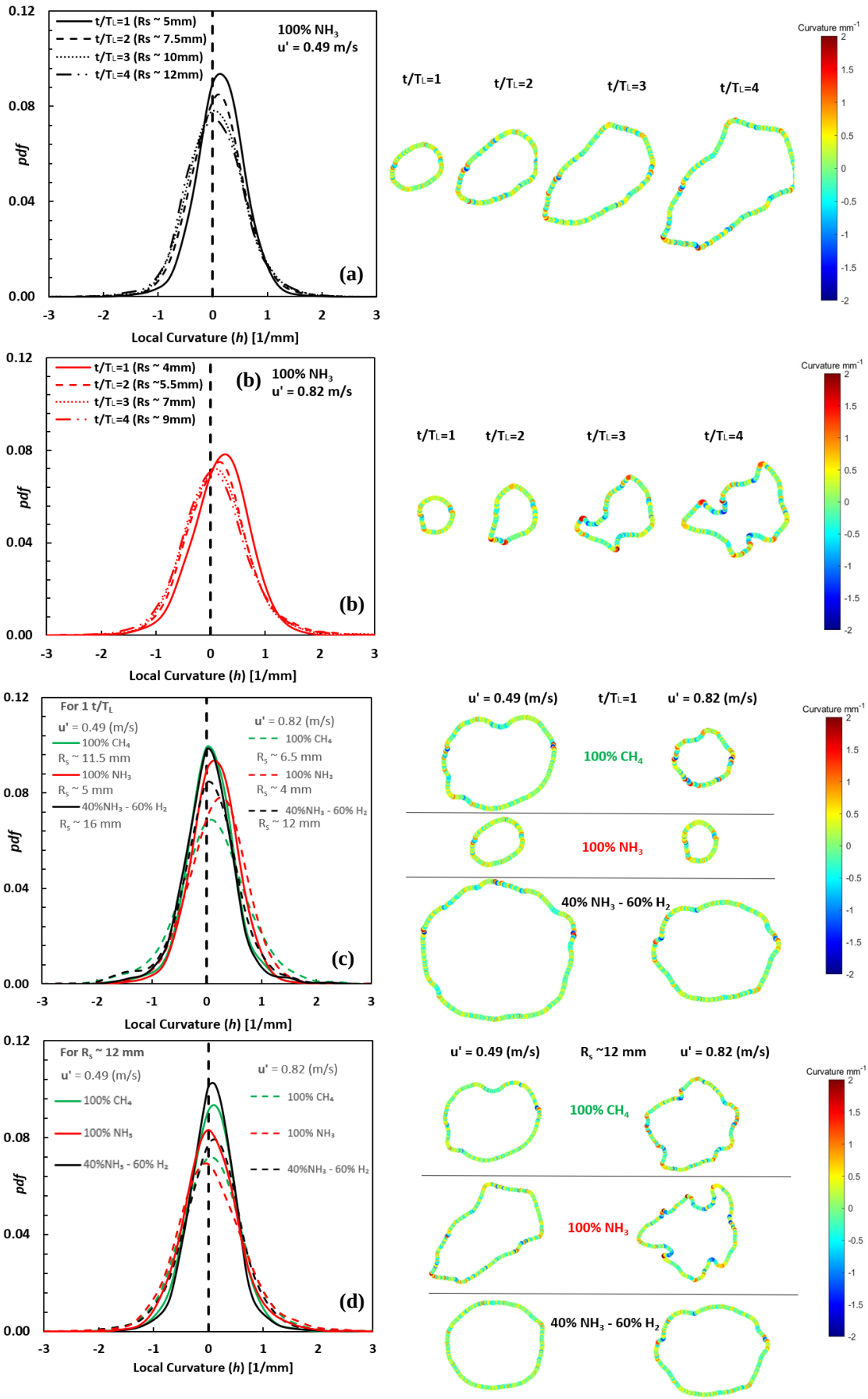

Figure 3: Flame contour sequences and curvature pdfs; 100% NH_3 as a function of t/T_L for (a) u'=0.49 and (b) 0.82 (m/s); 100% CH_4, 100% NH_3, 40% - 60% NH_3/H_2 (c) for $t/L_T = 1$ (d) for R_s = 12 mm.

The values of W against the flame radius is plotted for u' = 0.49 and 0.82 m/s, in Figures 2(a) and (b), respectively. Results suggest that at lowest turbulence intensity, all blends exhibit similar values, alluding to flame contours displaying similar structure size. As the turbulence increases, all blends exhibit a sharper increase in wrinkling ratio, as expected, since an increase in u' leads to decreasing the smallest turbulence scales, consequently enhancing wrinkling. Furthermore, as highlighted in [20], the squared turbulent flame brush thickness, δ_T^2 estimated by $\delta_T = (u'T_L)^{1/2}\, t^{1/2}$, with t, measured from the ignition event (see Table 1), increases with u' and time (or radius), enhancing wrinkling and then increasing the flame speed. This appears to corroborate with the flame wrinkling evolution. Nevertheless, the pure NH_3/ air and the blends with only 10% H_2 and 30% CH_4 displayed a much greater increase in wrinkling flame ratio, with this wrinkling intensification decreasing with higher CH_4 and H_2 content.

To better understand this intensified wrinkling, Figure 3 illustrates flame contours and corresponding flame curvature probability density functions (pdfs) from the experiments. The flame contours are colour coded, with blue, red and green, signifying negative curvature, positive curvature, or curvatures close to zero, respectively. Note that the example flame contours corresponds to a single experiment, whilst the pdfs are averaged over multiple experiments at either a set eddy turn over time (t/T_L) or equivalent flame radius (R_s).

The pdf's of curvature for 100% NH_3 at u' = 0.49 and 0.82 m/s at various t/T_L are illustrated in Fig. 3 (a) and (b), respectively. Clearly the mean curvatures are positive for all t/T_L with mean curvature moving closer to zero as the flame kernel grows (and deviates more and more from a spherical shape as observable from the flame contours), with this most apparent at u' = 0.82 m/s. The distribution of curvature widens slightly as the u' is increased, both on the negative and positive side, indicating increased wrinkling. However, this widening remains small, in comparison to the sharp increase in wrinkling ratio observed in Figure 2. It is also noted that the maximum of the pdf decreases with increasing u' and t/T_L.

To enhance clarity, only results for pure NH_3, pure CH_4 and NH_3/H_2 (40-60%) are plotted in Fig. 3 (c – d) for both u', since the blends respectively demonstrated high, moderate and low wrinkling ratios, respectively, as illustrated in Figure 2. The pdf's of curvature at t/T_L =1 for the investigated blends are illustrated in Figure 3 (c) alongside typical flame contours. It is noted that at lowest u', both CH_4 and 40/60 NH_3/H_2 flames exhibit near identical pdfs, reflecting a global laminar structure, as illustrated by their corresponding flame contours. On the other hand, pure NH_3 flame exhibits a distribution of curvature shifted towards positive curvatures. All the blends display similar dispersion pdf curvature profiles after 1 eddy turn over time, at lowest turbulent intensity. This is in good agreement with the wrinkling ratio illustrated in Figure 2 (a) with CH_4 (R_s~11.5mm) NH_3 (R_s~5 mm), 40/60 NH_3/H_2 (R_s~16mm), all exhibiting wrinkling ratios ~ 1.3. An increase in the turbulence intensity results in a widening of the curvature distribution for all the blends, with CH_4 exhibiting the greatest spread followed by pure NH_3. The pure NH_3 maintains a pdf curvature profile shifted towards positive values. Although both pure NH_3 and CH_4 exhibit similar Lewis number (Le) values ~ 1 (Le = 0.96 & 1.01, respectively) and similar stretch behavior (positive Markstein Length, see Table 1), they display different curvature pdfs. It is noted that both these mixtures are located within the thin reaction zone regime on the Borghi diagram, however, pure NH_3 crosses the Damköhler limit = 1 (Da < 1), with the CH_4 flames located at Da > 1. Furthermore, the NH_3 flames exhibits a much larger laminar flame thickness (δ_L) than CH_4, (~ 4 times bigger, see Table 1), which may potentially result in different eddy turbulent-flame interaction, reflected by different local curvature profiles.

Comparison at $t/T_L = 1$, results in flame kernels of very different sizes due to the greatly different burning rates of the investigated blends. As such, for comparison purposes, Figure 3 (d) illustrates the pdf's of curvature at a fixed surface radius equivalent, R_s = 12 mm. It is worth underling that the pure NH_3 flame has experienced multiple t/T_L (~4) in comparison to the CH_4 and 60/40 NH_3/H_2 flames at R_s=12 mm. As expected the mean curvatures are positive for all the blends; with 60/40 NH_3/H_2 blend displays the greatest mean zero curvature, and 100% NH_3 the least, irrespective of the u'. Increased turbulence intensity results in a widening of the distribution, with NH_3 displaying the greatest spread, and the NH_3/H_2 the least, analogous to the wrinkling trend illustrated in Figure 2.

Conclusions

To enhance knowledge about turbulent-flame interaction for ammonia flames, global and local flame structure analysis was conducted upon spherically expanding flames, for different stages of flame development and ammonia blends containing up to 60% CH_4 and H_2 at two turbulent intensities. From the flame morphology point of view, it was observed that NH_3 flame geometry kept evolving with time, losing its 'global laminar' flame kernel at very early stages of flame propagation, going onto develop tube or strip like structures. This behaviour was opposite to that observed for CH_4 flame, as the flame front reaches a certain geometry after a time of development, maintained over time. The wrinkling ratio was found to increase with both increasing ammonia fraction and turbulent intensity, in good agreement with observed flame contours and geometries. The flame curvature probability density functions of the various blends were investigated at various eddy turn-over times and equivalent surface radii. Results show that the local curvature pdf of the pure NH_3/air flame shifts towards greater local zero curvature with increasing eddy turn

over time. In general, the mean curvature is positive for all examined flames, with an increase in turbulence intensity resulting in widening of the curvature distribution, both on the negative and positive side. It is noted that after experiencing the same turbulent spectrum (1 eddy over time), the CH_4 and NH_3 flames exhibit different pdf curvature profiles, with differences growing with increasing turbulent intensity. NH_3 maintains a pdf curvature profile shifted towards positive values, although both CH_4 and NH_3 exhibit similar thermo-diffusive and laminar stretch related behavior as well as both being located in the same turbulent combustion regime.

Finally, although there are analogous trends the measured wrinkling ratios and the distribution curvature profiles, with greater distribution reflecting greater wrinkling, further work is required better understand the wrinkling evolution of NH_3 based flames.

Acknowledgements
This project has received funding from the European Union's Horizon 2020 research and innovation programme agreement No. 884157. Also, this research has received funding from the French Government's ''Investissement d'avenir'' program: 'Laboratoire d'excellence CAPRYSSES'' (Grant N. ANR-11-LABX-0006-01).

References

[1] T. Letcher, Climate Change: Observed Impacts on Planet Earth, 2nd ed., Elsevier, 2015.

[2] W. S. Chai, Y. Bao, P. Jin, G. Tang, L. Zhou, A review on ammonia, ammonia-hydrogen and ammonia-methane fuels, Renew. Sust. Energ. Rev. 147 (2021).

[3] H. Kobayashi, A. Hayakawa, K. A. Somarathne, E. C. Okafor, Science and technology of ammonia combustion, Proc. Combust. Inst. 37 109–133.

[4] N. A. Hussein, A. Valera-Medina, A. S. Alsaegh, Ammonia- hydrogen combustion in a swirl burner with reduction of NOx emissions, Enrgy. Proced. 158 (2019) 2305–2310.

[5] A. Hayakawa, Y. Arakawa, R. Mimoto, K. D. K. A. Somarathne, T. Kudo, H. Kobayashi, Experimental investigation of stabilization and emission characteristics of ammonia/air premixed flames in a swirl combustor, Int. J. Hydrogen Energy 42 (2017) 14010–14018.

[6] C. Lhuillier, P. Brequigny, F. Contino, C. Mounaïm-Rousselle, Experimental study on ammonia/hydrogen/air combustion in spark ignition engine conditions, Fuel 269 (2020) 117448.

[7] C. Lhuillier, P. Brequigny, F. Contino, C. Mounaïm-Rousselle, Experimental investigation on ammonia combustion behavior in a spark-ignition engine by means of laminar and turbulent expanding flames, Proc. Combust. Inst. 38 (2021) 6671–6678.

[8] R. Kanoshima, A. Hayakawa, T. Kudo, E.C. Okafor, S. Colson, A. Ichikawa, T. Kudo, H. Kobayahsi, Effects of initial mixture temperature and pressure on laminar burning velocity and Markstein length of ammonia/air premixed laminar flames, Fuel 310 (2022) 122149.

[9] C. Lhuillier, P. Brequigny, N. Lamoureux, F. Contino, C. Mounaïm-Rousselle, Experimental investigation on laminar burning velocities of ammonia/hydrogen/air mixtures at elevated temperatures, Fuel 263 (2020) 116653.

[10] A. Hayakawa, T. Goto, R. Mimoto, Y. Arakawa, T. Kudo, H. Kobayashi, Laminar burning velocity and Markstein length of ammonia/air premixed flames at various pressures, Fuel 159 (2015) 98–106.

[11] A. Ichikawa, A. Hayakawa, Y. Kitagawa, K. D. Kunkuma Amila Somarathne, T. Kudo, H. Kobayashi, Laminar burning velocity and Markstein length of ammonia/hydrogen/air premixed flames at elevated pressures, Int. J. Hydrogen Energy 40 (2015) 9570–9578.

[12] A. M. Elbaz, S. Wang, T. F. Guiberti, W. L. Roberts, Review on the recent advances on ammonia combustion from the fundamentals to the applications, Fuel Commun. 10 (2022) 100053.

[13] S. Zitouni, P. Brequigny, C. Mounaim-Rousselle, Turbulent Flame Speed and Morphology of Pure Ammonia flames and Blends with Methane or Hydrogen, Proc. Combust. Inst. (2022)

[14] R. Ichimura, K. Hadi, N. Hashimoto, A. Hayakawa, H. Kobayashi, O. Fujita, Extinction limits of an ammonia/air flame propagating in a turbulent field, Fuel 246 (2019) 178–186.

[15] B. Galmiche, N. Mazellier, F. Halter, F. Foucher, Turbulence characterization of a high-pressure high-temperature fan-stirred combustion vessel using LDV, PIV and TR-PIV measurements, Exp. Fluids 55 (2014)

[16] P. Brequigny, F. Halter, C. Mounaïm-Rousselle, Lewis number and Markstein length effects on turbulent expanding flames in a spherical vessel, Exp. Therm. Fluid Sci. 73 (2016) 33–41.

[17] B. Renou, A. Boukhalfa, D. Puechberty, M. Trinité, Effects of stretch on the local structure of freely propagating premixed low-turbulent flames with various lewis numbers, Proc. Combust. Inst. 27 (1998) 841-847.

[18] D. Bradley, M. Lawes, K. Liu, M. S. Mansour, Measurements and correlations of turbulent burning velocities over wide ranges of fuels and elevated pressures, Proc. Combust. Inst., 34 (2013) 1519–1526.

[19] C. K. Law, Combustion Physics, Cambridge: Cambridge University Press, 2006.

[20] J. F. Driscoll, Turbulent premixed combustion: Flamelet structure and its effect on turbulent burning velocities, Prog. Energy Combust. Sci., 34(2008) 91–134.